DEVELOPMENT AND ASSESSMENT OF AN X-RAY FLUORESCENCE SYSTEM FOR *IN VIVO* STUDIES

by

WAN SALWANI JAAFAR

Thesis submitted in fulfilment of the requirements for the Degree of Doctor of Philosophy

June 2009

ACKNOWLEDGEMENTS

Praise is to Allah the Lord of the Universe.

It is a pleasure to acknowledge indebtedness to the many individuals that made this study possible. First and foremost, I wish to express my sincere thanks to my main supervisor, Professor Dr. Ahmad Shukri Mustapa Kamal for his kind guidance, generous support, constant encouragement and invaluable advice over the course of my study. My sincere thanks also go to my co-supervisor, Dr. Sabar Bauk for his support, encouragement, helpful suggestions in working on the experiments and also for his invaluable criticisms and suggestions right from the early drafts of this thesis.

I would like to express my gratitude to Universiti Teknologi Mara for the financial support throughout my study and also to the Dean, Faculty of Applied Sciences, UiTM and the Campus Director, UiTM Perlis for their permission to release me for my study leave.

I would like to thank the Dean and staff of the School of Physics, Universiti Sains Malaysia for providing me with substantial support, most notably Mr. Azmi Omar, Mr. Azmi Abdullah and Mr. Yahya for their technical assistance in the laboratory and assuring that all my supplies was there when they were needed. I am greatly indebted to my colleagues in UiTM Perlis; Professor Dr. Khudzir, Sabiha Hanim, Assoc. Prof Zurina, Zaini and Rohaiza who shared with me their expertise in analytical chemistry and Assoc. Prof. Norsila for the identification of the marine

specimens. I also would like to thank current and former graduate students of the Medical Physics group; especially to Dr Eid for sharing his expertise in the Monte Carlo simulations and taking time to engage in open scientific discussions with me and Dr Bassam for his guidance on using the X-ray generator during the initial stage of experimentation. In addition, I would like to thank my friends; Aishah, Dr Rini and Ramzun who could always be counted on for diversions and also for making my life in the laboratory and my stay in the International House joyful.

Special thanks go to my parents, Jaafar and Wan Halimah for their motivation, prayers and moral support and to my children; Firdaus, Nadiah, Faiz, Najwa, Farhan and Nuha and also daughter-in-law, Nik Farhana for their understanding and patience while mum was away from home. I also would like to thank my siblings; Sakinah, Dr. Suhaimi, Salmiah, Saidi and Salmizi for their encouragement throughout my study.

Finally, the greatest thanks go to my beloved husband, Mohamad Nadzam Yaacob for giving me the permission to pursue my studies, for his love and emotional support, for his patience and understanding, for his advices and encouragement, and also for his sacrifices in taking the responsibility of the whole family throughout this endeavour. This thesis is dedicated especially to him.

TABLE OF CONTENTS

LIST OF TABLES

LIST OF FIGURES

LIST OF PLATES

LIST OF SYMBOLS

α	alpha
β	beta
γ	gamma
θ	theta
ϕ	phi
μ	micro
m	milli
k	kilo
λ	decay constant
Z	atomic number
A	mass number
σ	standard deviation
ρ	density
E_0	incident photon energy
E_{BE}	binding energy
E_S	scattered photon energy
μ_l	linear attenuation coefficient
μ_m	mass attenuation coefficient

LIST OF ABBREVIATIONS

Bq	becquerel
CdTe	cadmium telluride
CdZnTe	cadmium zinc telluride
EGS	electron gamma shower
ETRAN	electron transport
eV	electron volt
GHz	gigahertz
Gy	gray
HVL	half value layer
HPGe	high purity germanium
ITS	integrated tiger system
IAEA	International Atomic Energy Agency
kVp	kilovolt peak voltage
Ge(Li)	lithium drifted germanium
Si(Li)	lithium drifted silicon
L	litre
LEGe	low energy germanium
MDL	minimum detectable limit
HgI	mercury iodide
MCNP	Monte Carlo N-Particle
MCNP5	Monte Carlo N-Particle version 5
NAA	neutron activation analysis
ppm	parts-per-million

RAM	random access memory
SDD	sample-to-detector distance
Sv	sievert
NaI(Tl)	sodium iodide thallium
SSD	source-to-sample distance
sr	steradian
XRF	X-ray fluorescence

LIST OF APPENDICES

LIST OF PUBLICATIONS & SEMINARS

Jaafar, W. S. and Shukri, A., 2006. Monte Carlo Simulations for *in vivo* Analysis of Arsenic Using X-Ray Fluorescence. In: *5th National Seminar on Medical Physics: Globalization of Physics in Health and Medical Sciences*. Kuala Lumpur, Malaysia 14-15 December 2006. Malaysian Association of Medical Physics: Kuala Lumpur.

Jaafar, W. S. and Shukri, A., 2006. Monte Carlo Simulations for *in vivo* Analysis of Arsenic Using X-Ray Fluorescence, *NSMP 2006 Proceedings,* pp.68-74.

PEMBANGUNAN DAN PENILAIAN SATU SISTEM

PENDARFLUORAN SINAR-X BAGI KAJIAN "*IN VIVO*"

ABSTRAK

Pendarfluor sinar-X (XRF) yang merupakan satu teknik analisis unsur piawai dikaji bagi tujuan pengukuran unsur "*in vivo*". Satu sistem XRF yang terdiri daripada sumber pengujaan, sampel dan sistem pengesan pada geometri 90° dimaju dan dioptimumkan dengan kaedah simulasi menggunakan kod Monte Carlo Zarah-N versi 5 (MCNP5). Bagi kegunaan optimum, sudut geselan sampel adalah 15° dan jarak bagi sumber-sampel dan sampel-pengesan adalah pada nilai minimum. Bagi penentusahan eksperimen, satu sistem fizikal hampir serupa dengan sistem simulasi disediakan di makmal Biofizik, Pusat Pengajian Sains Fizik, USM. Sistem tersebut terdiri daripada tiub sinar-X, kolimator, sampel, pemerisaian, pengesan dan peralatan pemerolehan data. Ciri-ciri bagi sumber pengujaan dan pengesan pendarfluor sinar-X dikaji dengan analisis spektrum dilakukan menggunakan perisian penyuaian 'PeakFit'. Pengoptimuman dijalankan dan pengukuran eksperimen menunjukkan keputusan adalah selari dengan simulasi. Tentukuran yang dijalankan untuk arsenik didapati paras boleh kesan minimum adalah masing-masing (2.83 ± 0.01) μg/g dan (0.74 ± 0.02) μg/g bagi simulasi dan eksperimen. Bagi menentukan ketersauran lanjutan teknik kepada analisis berbilang unsur, lima unsur yang mempunyai kepentingan pemakanan dan toksikologi iaitu kromium, kobalt, selenium, strontium dan kadmium ditentukur dan analisis serentak unsur ditentukan dalam unsur duaan dan berbilang. Keputusan menunjukkan, perbezaan bagi kepekatan unsur yang diukur adalah masing-masing dalam julat 0.1 hingga 7.1% dan 0.3 hingga 12.3%

bagi unsur duaan dan berbilang dibandingkan dengan sampel satu unsur. Bagi melanjutkan penilaian keupayaan teknik tersebut, analisis unsur dalam invertebrat marin Malaysia umum dijalankan. Keputusan bagi kepekatan arsenik dan selenium adalah dalam magnitud yang sama dibandingkan dengan yang didapati melalui teknik Analisis Pengaktifan Neutron (NAA). Julat kepekatan bagi arsenik, selenium, strontium dan kadmium yang diperolehi adalah sebanding dengan yang diperolehi bagi spesis marin dari kajian literatur yang lain.

DEVELOPMENT AND ASSESSMENT OF AN X-RAY FLUORESCENCE SYSTEM FOR *IN VIVO* STUDIES

ABSTRACT

X-ray fluorescence (XRF), which is a standard elemental analysis technique, was investigated for the purpose of measuring elements *in vivo*. An XRF system comprising of an excitation source, sample and a detection system in a 90° geometry was developed and optimized by simulations using the Monte Carlo code, Monte Carlo N-Particle version 5 (MCNP5). For optimal use, the grazing angle of the sample is at 15° and the source-to-sample distance (SSD) and sample-to-detector distance (SDD) were at minimum values. For experimental verification, a physical system almost similar to the simulated system was set up at the Biophysics Laboratory, School of Physics, USM. The system comprises of an X-ray tube, collimators, sample, shielding, a detector and data acquisition equipments. The characteristics of the excitation source and the fluorescent X-ray detector were investigated with spectral analysis performed using the PeakFit fitting software. Optimizations were carried out and experimental measurements showed that the results agreed with that obtained by simulations. Calibration for arsenic was performed with the minimum detectable level by simulation and experimentation determined to be (2.83 ± 0.01) μg/g and (0.74 ± 0.02) μg/g respectively. To determine the feasibility of extending the technique to multi-elemental analysis; another five elements of nutritional and toxicological interest, namely chromium, cobalt, selenium, strontium and cadmium were calibrated and then simultaneously determined in dual and multi-elemental analysis. Results showed that, compared to single element samples, the differences of the measured concentrations of the

elements ranges from 0.1 to 7.1% and 0.3 to 12.3% in dual and multi-elemental samples respectively. To further evaluate the capacity of the technique, analysis of the elements in common Malaysian marine invertebrates were performed. Results for arsenic and selenium concentrations as compared with that obtained from another technique, Neutron Activation Analysis (NAA) showed that the concentrations were within the same order of magnitude. The ranges of arsenic, selenium, strontium and cadmium concentrations obtained were comparable to that obtained for marine species in other studies in the literature.

CHAPTER ONE

INTRODUCTION

1.1 Introduction

XRF has become a powerful and portable analytical tool in many fields. Fluorescence, or the generation of secondary radiation, is accomplished by a two-step process. In the first step, a high energy particle such as a photon, a proton or an electron strikes an atom and knocks out an inner-shell electron (photoelectric effect). The second step is readjustment in the atom almost immediately (10^{-12} to 10^{-14} s) by filling the inner-shell vacancy with one of the outer-shell electrons and the simultaneous emission of an X-ray photon. The first step uses up the energy of the incident quantum, and in the second step energy is emitted as the characteristic X-ray photon.

The technology works by irradiating samples of materials using X-rays without destroying the analysed material. The material emits radiation, which has an energy characteristic of the atoms present. Analysis by XRF consists of determining the content of specific elements in a sample by producing vacancies in the electronic structures and analysing the photons emitted as a consequence. At the same time, it can identify a vast number of elements simultaneously, making it an excellent way to "fingerprint" all kinds of materials.

1.2 Applications of X-ray Fluorescence

The great flexibility and range of the various types of X-ray spectrometers coupled with the development in X-ray detectors has established the XRF method as a powerful technique in a number of applications, including:

a) Geology and mineralogy; for the analysis of minerals (Pinetown *et al.*, 2007, Siyanbola *et al.*, 2004), rocks (Tarasov *et al.*, 1998), ore (Devan *et al.*, 1997, Herrera Peraza *et al.*, 2004), soils (Mc Donald *et al.*, 1999), silts and sediments (Zachara *et al.*, 2004) and the heavy metals measurement in rock phosphates (Hayumbu *et al.*, 1995).

b) Ecology and environmental management; for the analysis of aerosols (Devan *et al.*, 1997); pollution of water (Marques *et al.*, 2003), soil (Krishna and Govil, 2007) and air particle (Suarez *et al.*, 2004); lead monitoring in lead-based industrial areas (Herman *et al.*, 2006) and soil samples (Markey *et al.*, 2008); and the assessment of marine pollution (Woelfl *et al.*, 2006) and heavy metals in lake sediments (de Vives *et al.*, 2007).

c) Archaeology and forensics; in the analysis of ancient pottery (Papachristodoulou *et al.*, 2006), Chinese jades (Casadio *et al.*, 2007), ceramics (Cechak *et al.*, 2007), porcelain (Yu and Miao, 1997) and glass (Jembrih-Simburger *et al.*, 2004); metal artifacts (Araujo *et al.*, 2004, Fikrle *et al.*, 2006) and coins (Linke *et al.*, 2004); human bones of ancient populations (Rebocho *et al.*, 2006) and the investigation of paintings (Szokefalvi-Nagy *et al.*, 2004) and other works of art (Cesareo *et al.*, 1999).

d) Industry; for the analysis of trace elements in a metal matrix for the assessment of radiation damage of core components in a nuclear power plant (van Aarle *et al.*, 1999), elemental composition of chromites ore in the

ceramic industry (Sanchez-Ramos *et al.*, 2008), elemental analysis in lubricants (Schramm, 2002), determination of wear metals in engine oil (Yang *et al.*, 2003) and used lubricating oils (Arikan *et al.*, 1996), concentration of sulphur in the products of the petroleum industry (Christopher *et al.*, 2001, Miskolczi *et al.*, 2005) and the analysis of trace elements in coal (Suarez-Fernandez *et al.*, 2001), waste material (Akinci and Artir, 2008) and cement factory raw material (Polat *et al.*, 2004).

e) Clinical and biological; for *in vivo* studies such as measurement of lead in bone (Somervaille *et al.*, 1985); studies on aquatic species such as the analysis of muscles and livers of freshwater fish (Wagner and Boman, 2004), studies on how metals accumulate and redistribute during fertilization and embryonic developments of the African clawed frog (Popescu *et al.*, 2007); studies of plants (Richardson *et al.*, 1995), mushrooms (Carvalho *et al.*, 2005), plants having medicinal properties (Ekinci *et al.*, 2004) and plant materials such as the analysis of fruit juice (Bao *et al.*, 1999) and spices (Al-Bataina *et al.*, 2003, Jayasekera *et al.*, 2004).

1.3 Scope of Work

XRF has been an established technique for the measurement of toxic and essential trace elements *in vivo* (Borjesson *et al.*, 1998, Chettle, 2005). This study involves the designing, developing and assessing of an XRF system and will be restricted to applications for *in vivo* studies.

With the help of faster computers, simulation is becoming more and more important in many fields of design and analysis due to the several advantages of

simulations compared to experimental studies. Taking this into account, computer simulations, particularly the Monte Carlo N-Particle version 5 (MCNP5) code will be used. Different parameters in the simulation will be changed and the effect of these changes on the performance of the XRF system will be investigated. The system will be optimized and calibrated by using both computer simulations and experimental methods.

1.4 Research Objectives

The objective of this research is to use computer simulations and experimental analysis to examine photon interactions associated with *in vivo* XRF measurement of arsenic. This investigation is designed to determine the feasibility of extending the technique of XRF of arsenic to multi-elemental analysis of another five elements particularly, chromium, strontium, cadmium, cobalt and selenium where their atomic number, Z ranges from Z = 24 to Z = 48.

During the course of the investigation attempts were made:

a. To develop an arsenic XRF system with Monte Carlo simulation and experimental verification.

b. To calibrate the X-ray intensity with concentration for arsenic and the other elements by both methods.

c. To acquire information concerning the feasibility of obtaining concentration for two elements and six elements simultaneously for *in vivo* measurements and

d. To apply the XRF system to determine the concentration of elements of interest in common Malaysian marine invertebrates *in vivo* and to compare

with those obtained by using the method of neutron activation analysis (NAA).

1.5 Thesis Organisation

In this thesis, an XRF system with the potential for *in vivo* studies is presented. The XRF system was developed and optimized by computer simulations using the Monte Carlo N-Particle Version 5 (MCNP5) code and also by experimentation.

Appropriate parameters had to be identified and understood in terms of how the parameters affect the output counts of the XRF system. With this in mind, Chapter 2 contains the theoretical background and characterisation parameters which are related and important to the XRF system. The descriptions about MCNP5 which are relevant to the system are also presented. Chapter 3 contains a description of the characteristics of each component of the XRF system and Chapter 4 contains a description of how those parameters were optimized by both MCNP5 and experimentation and also the calibration of the XRF system for arsenic. Chapter 5 contains the extension of the XRF system for five other elements of interest which includes elemental calibration and the analysis of two and six elements simultaneously. The application of multi-elemental analysis on common Malaysian marine invertebrates was described and with the analysis of data obtained, the elements concentrations were evaluated. Comparisons made with the method of neutron activation analysis showed that the XRF system has the potential to be used for *in vivo* studies.

CHAPTER TWO

THEORETICAL BACKGROUND

2.1 Introduction

X-rays are electromagnetic radiation with their region lying between 0.01 and 10 nm (0.1 to 100 keV) in the electromagnetic spectrum, that is between the γ-region at the short-wavelength or high-energy side and the ultraviolet region at the long-wavelength or low-energy side. However, these boundaries are not clearly defined.

2.2 Interactions of X-rays with Matter

When a beam of X-ray photons passes into an absorbing medium, the process of collision between one photon and some electrons in the medium produces scattered radiation and the setting in motion of a high speed electron. The process of interaction is by four distinct mechanisms known as Rayleigh scattering, Compton scattering, photoelectric absorption and pair production.

2.2.1 Rayleigh Scattering

An incident X-ray photon can interact with an electron and be deflected (scattered) with no loss of energy. The process which is also known as coherent or elastic scattering occurs by temporarily raising the energy of the electron although the electron remains bound to the nucleus. The electron returns to its initial energy level by emitting an X-ray photon of equal energy but with a slightly different direction, as illustrated in Figure 2.1A. No ionisation takes place and no energy is lost in Rayleigh scattering. Rayleigh scattering occurs at all X-ray energies, however

it never accounts for more that 10% of the total interaction processes in diagnostic radiology (Dendy and Heaton, 2000). This type of scattering is dependent approximately on Z^2 and of importance in analytical X-ray fluorescence because of its contribution to the general background (Biran-Izak and Mantel, 1994).

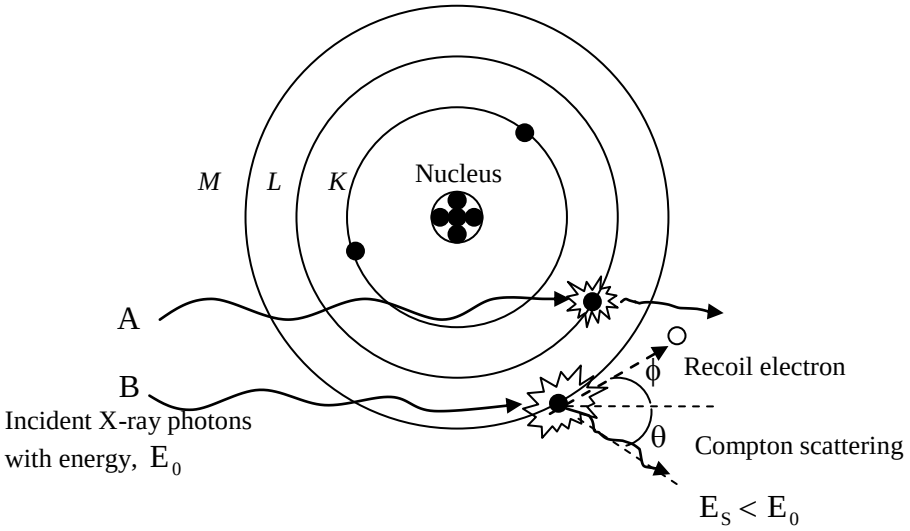

Figure 2.1: Illustrative summary of (A) Rayleigh scattering and (B) Compton scattering.
(Seibert and Boone, 2005).

2.2.2 Compton Scattering

Compton scattering is an inelastic interaction between an X-ray photon of energy E_0 that is much greater than the binding energy of an atomic electron (in this situation, the electron is essentially regarded as "free" and unbound). Partial energy transfer to the electron causes a recoil and removal from the atom at an angle, ϕ. The remainder of the energy E_S is transferred to a scattered X-ray photon with a trajectory of angle θ relative to the trajectory of the incident photon as illustrated in Figure 2.1B. The scattered photon may travel in any direction that is, scattering through any angle θ from 0° to 180°; but the recoil electron may only be directed

forward relative to the angle of the incident photon that is the angle ϕ lies from 0° to ~90°. Due to the physical requirements to preserve both energy and momentum, the energy of the scattered photon relative to the incident photon for a photon scattering angle θ is given by the Compton relations:

$$\frac{E_S}{E_0} = \frac{1}{1 + \frac{E_0}{511\ \text{keV}}(1 - \cos\theta)} \tag{2.1}$$

where 511 keV is the energy equal to the rest mass of the electron and E_0 and E_S are in keV.

Compton scattering is independent of atomic number and it decreases with increase in energy. The most important consequence of Compton scattering is the appearance of scattered photons of lower energy than the incident photon beam, which may cause overlap and high background effects in the XRF spectra.

2.2.3 Photoelectric Absorption

Photoelectric absorption involves the interaction of an incident X-ray photon with an inner shell electron in the absorbing atom that has a binding energy similar to but less than the energy of the incident photon. The incident X-ray photon transfers its energy to the electron and results in the ejection of the electron from its shell (usually the *K* shell) with a kinetic energy equal to the difference of the incident photon energy, E_0, and the electron shell binding energy, E_{BE} as shown in Figure 2.2. For clarity, only one line is indicated in each shell.

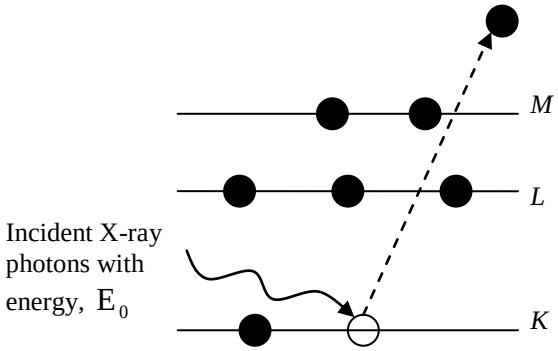

Figure 2.2: Photoelectric absorption.
(Als-Nielsen and Mc Morrow, 2001).

The vacated electron shell is subsequently filled by an electron from an outer shell with less binding energy, e.g. from the *L* shell as in Figure 2.3A or the *M* shell as in Figure 2.3B, producing a characteristic X-ray equal in energy to the difference in electron binding energies of the source electron shell and the final electron shell.

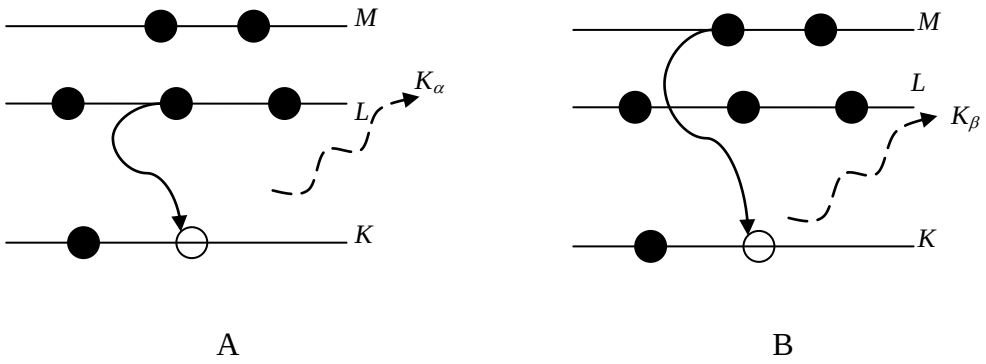

Figure 2.3: Fluorescence X-ray emission of (A) K_α and (B) K_β.
(Als-Nielsen and Mc Morrow, 2001).

Alternatively, the energy released by an electron hopping from the *L* shell to the hole in the *K* shell can be used to expel yet another electron from one of the outer shells, as illustrated in Figure 2.4. This secondary emitted electron is called an Auger electron, named after the French physicist who first discovered the process.

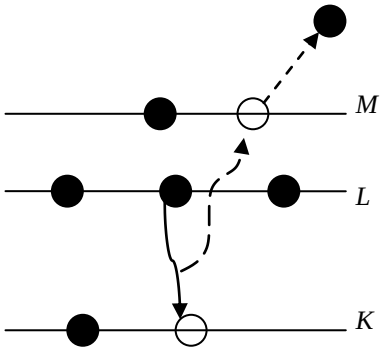

Figure 2.4: Auger electron emission.
(Als-Nielsen and Mc Morrow, 2001).

If the incident photon energy is less than the binding energy of the electron, the photoelectric interaction cannot occur, but if the X-ray energy is equal to the electronic binding energy $(E_0 = E_{BE})$, the photoelectric effect becomes energetically feasible and a large increase in attenuation occurs. As the incident photon energy increases above that of the electron shell binding energy, the likelihood of photoelectric absorption decreases at a rate proportional to E^{-3}.

The *K* absorption edge refers to the sudden jump in the probability of photoelectric absorption when the *K*-shell interaction is energetically possible. Similarly, the *L* absorption edge refers to the sudden jump in photoelectric absorption occurring at the *L*-shell electron binding energy (at much lower energy). Actually, the *K* absorption edge is approximately the sum of the *K, L* and *M* line energies, and the *L* absorption edge energy is approximately the sum of the *L* and *M* line energies of the particular element.

The characteristic X-rays are labelled as *K, L* or *M* to denote the shells they originated from. The designations α, β or γ is made to mark the X-rays that originated from the transitions of electrons from the higher shells. Hence, a K_α X-ray

is produced from a transition of an electron from the *L* to the *K* shell, and a K_β X-ray is produced from a transition of an electron from the *M* to the *K* shell. Within the shells there are multiple orbits of higher and lower binding energy electrons as shown in Figure 2.5, hence a further designation is made as α_1, α_2, or β_1, β_2 etc. to denote transitions of electrons from these orbits into the same lower shells. After photoelectric interaction, ionisation of the atom occurs and a free (photo) electron and a positively charged atom are produced.

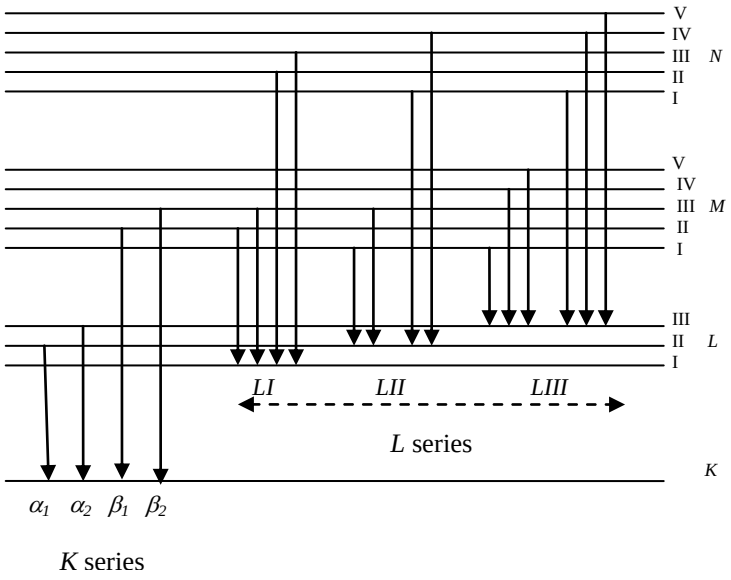

Figure 2.5: Energy level diagram and electronic transition.
(Pinta, 1978).

2.2.4 Pair Production

Pair Production can occur when an incident X-ray has energy greater than 1.022 MeV, which represents the rest mass energy equivalent of 2 electrons;

$$E = 2 m_0 c^2 \qquad (2.2)$$

where (m_0) is the rest mass of the electron (= 9.11×10^{-31} kg) and

(c) is the speed of light (= 3.0×10^8 m/s).

The interaction of the incident photon with the electric field of the nucleus results in the production of an electron (e^-) and a positron (e^+) pair, with any photon energy in excess of 1.022 MeV being transferred to the kinetic energy of the e^-/e^+ pair equally. Interestingly, ionisation of the atom does not occur, although charged particles are formed and their kinetic energy can result in subsequent ionisation within the local area. Once the positron expends its kinetic energy, it will combine with any available electron and produce annihilation radiation, resulting from the conversion of the rest mass energies of the e^-/e^+ pair into (nearly) oppositely directed 511 keV photons as shown in Figure 2.6. The probability of a pair production which is commonly given the symbol π, increases with energy above 1.022 MeV (Seibert and Boone, 2005).

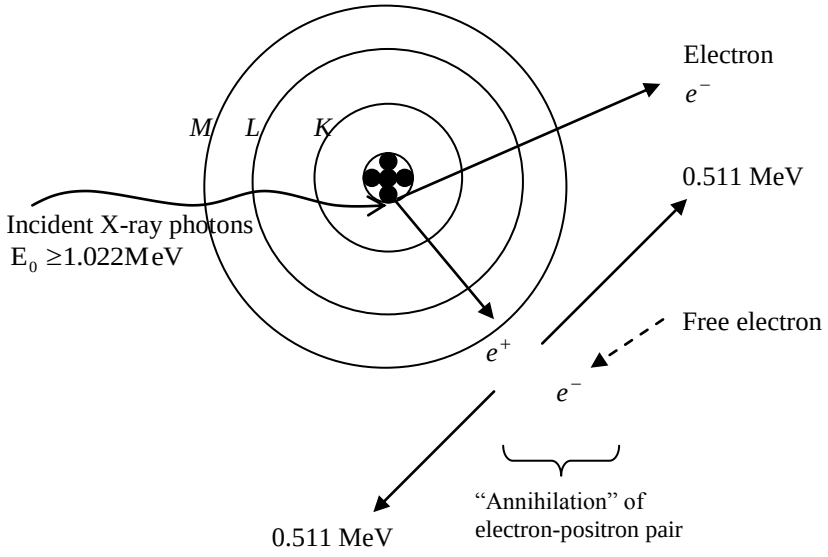

Figure 2.6: Illustration of pair production.

2.3 Attenuation

The interaction processes combine to attenuate the incident photon beam as it passes through matter through the removal of X-ray photons from the X-ray beam,

therefore decreasing its intensity, either by absorption or scattering events. The amount of decrease in intensity of the X-ray beam depends upon the depth of penetration or thickness, x and linear attenuation coefficient, μ_l which is a characteristic of the material, that is

$$I = I_0 \ e^{-\mu_l x} \tag{2.3}$$

where (I_0) and (I) are the initial and final X-ray beam intensities respectively.

The unit of thickness is commonly expressed in cm, so the corresponding unit of μ_l is cm^{-1}, and μ_l represents the probability of attenuation per cm of a material. The total linear attenuation coefficient is the sum of the linear attenuation coefficients for the individual interaction mechanisms, as

$$\underset{\text{total}}{\mu_{total}} = \underset{\text{photoelectric effect}}{\mu_{PE}} + \underset{\text{Compton scattering}}{\mu_{CS}} + \underset{\text{Rayleigh scattering}}{\mu_{RS}} + \underset{\text{Pair production}}{\mu_{PP}} \tag{2.4}$$

At low X-ray energy, μ_{PE} dominates and $\mu \propto Z^4 E^{-3}$; at high energy, μ_{CS} dominates and $\mu \propto \rho$ and only at very high energy, that is greater than 1.022 MeV does μ_{PP} contribute. Therefore, interaction by pair-production does not occur in this study because the X-ray energy used is very much lower than 1.022 MeV. At a given photon energy, the linear attenuation coefficient can vary significantly for the same material if it exhibits differences in physical density. A classical example is water, water vapour and ice. The mass attenuation coefficient,

$$\mu_m = \frac{\mu_l}{\rho} \tag{2.5}$$

compensated for these variations by normalising the linear attenuation by the density of the material, ρ. In terms of μ_m, Equation 2.3 now becomes

$$I = I_0 \ e^{-\mu_m \rho x} \tag{2.6}$$

An interesting application of Equation 2.6 is to determine the depth of penetration of X-rays. The attenuation length is defined as the depth into the material where the intensity of the X-rays has decreased to about 37% or $\frac{1}{e}$ of its value at the surface. That is, $I = \left(\frac{1}{e}\right) I_0$, or $\frac{I}{I_0} = \frac{1}{e}$ where (e) sometimes called Euler's number or Napier's constant, is the base of natural logarithms, or $e \approx 2.7183$. Then, substituting into Equation 2.6;

$$\ln\left(\frac{1}{e}\right) = -\mu_m \rho x$$

$$-1 = -\mu_m \rho x$$

Hence $$x = \frac{1}{\mu_m \rho} \tag{2.7}$$

where (x) is also referred to as the "mean free path" of the X-rays. The mean free path is, as the name suggests, the average distance travelled by a photon before undergoing some form of interaction.

X-ray beams have a spectral distribution of energies. Hence a rule of thumb is often used which states that the average X-ray energy is approximately one-third of the maximum energy or kVp (Khan, 1984). Therefore, for an operating voltage of 45

kVp which has been used as the identical operating voltage and described in Section 5.4.2(c), the average energy is approximately 15 keV. For soft tissue (ICRU Four-Component) of density, ρ = 1 g/cm^3 and the mass attenuation coefficient at 15 keV is μ_m = 1.266 cm^2/g (N.I.S.T., 2005); plugging in the numbers into Equation 2.7, the mean free path, x = 0.79 cm.

2.4 Trace Elements

Some metals are naturally found in the body and are essential to human health. They normally occur at low concentrations and are known as trace metals. In high doses, they may be toxic to the body or produce deficiencies in other trace metals; for example, high levels of zinc can result in a deficiency of copper, another metal required by the body. Heavy or toxic metals are trace metals with a density at least five times that of water. As such, they are stable elements which mean that they cannot be metabolised by the body and they are bio-accumulative, that is, they passed up the food chain to humans. Once liberated into the environment through the air, drinking water, food, or countless human-made chemicals and products, heavy metals are taken into the body via inhalation, ingestion and skin absorption. If heavy metals enter and accumulate in body tissues faster than the body's detoxification pathways can dispose them, a gradual build-up of these toxins will occur. High-concentration exposure is not necessary to produce a state of toxicity in the body as heavy metals accumulate in body tissues and over time can reach toxic concentration levels. Thus there is a need to control their levels in human organs and tissues especially for occupationally and environmentally highly exposed persons. The distribution of trace elements within the body is often very non-uniform and are

usually found in specific organs such as iodine in the thyroid, lead in bone and cadmium and mercury in kidney cortex, etc.

2.5 XRF for *in vivo* studies

There are two main non-invasive techniques for *in vivo* studies, namely the XRF and neutron activation analysis (NAA). Compared to NAA, XRF has the advantage of being non-destructive, multi-elemental, fast and cost-effective. The analysis is said to be non-destructive in the sense that, at the end of it, most of the elements originally present in the sample are still there and chemically unchanged. The sample is therefore; to some extent available for further study should this be considered necessary or desirable.

The first XRF measurement *in vivo* was performed to measure iodine levels in the thyroid gland (Hoffer *et al.*, 1968). However, the most recognised and applied XRF technique is bone lead XRF measurements in humans. Measurements of lead *in vivo* began in 1971 (Ahlgren *et al.*, 1976, Ahlgren and Mattsson, 1979) using 122 and 136 keV photons from ^{57}Co for excitation of the lead *K* X-rays and a similar technique has also been used to estimate the lead concentration in children's teeth *in situ* (Bloch *et al.*, 1976). There are four different approaches for bone lead measurements which have been developed, namely:

a. A ^{109}Cd source that induces *K* XRF of lead stored in the tibia or some other bone was employed in a backscatter geometry (Green *et al.*, 1993, Kondrashov and Rothenberg, 2001, Somervaille *et al.*, 1985),

b. A ^{57}Co source that irradiated a subject's finger bone, and thus, fluorescence accumulated lead was used in a 90º geometry (Ahlgren *et al.*, 1976, Christoffersson *et al.*, 1984),

c. A ^{125}I source was used to irradiate the bone site and lead *L* X-rays were measured (Wielopolski *et al.*, 1983) and

d. An X-ray generator which utilises polarised radiation to induce *L* XRF of lead stored in bone (Wielopolski *et al.*, 1989).

Problems due to heavy elements accumulated in occupationally exposed subjects led to a number of studies on *in vivo* XRF. Besides lead, several other heavy elements, usually toxic, have also been successfully measured. *In vivo* XRF studies of uranium (O' Meara *et al.*, 1997), mercury (Borjesson and Mattsson, 1995), cadmium (Carew *et al.*, 2005, Popovic *et al.*, 2006) and gold (Shakeshaft and Lillicrap, 1993) that accumulate in bone have been reported and measurements of cadmium in the kidney (Ahlgren and Mattsson, 1981, Christoffersson and Mattsson, 1983) and liver (Borjesson *et al.*, 2000) were also measured. *In vivo* XRF measurement of mercury content in organs near a surface, such as the superficial tissues of the head and the limbs (Bloch and Shapiro, 1981) was also reported.

Studies of the uptake and kinetic behaviour of toxic elements unintentionally introduced into the body through medical procedures or as diagnostic agents also led to the *in vivo* XRF studies. Platinum-based drugs were a common choice in chemotherapy and gold salts have been used in treating rheumatoid arthritis patients. XRF was applied for the measurement of platinum in kidneys (Jonson *et al.*, 1988, Kadhim *et al.*, 2000) and tumour in the head and neck region (Ali *et al.*, 1998a) of

Cisplatin treated patients and measurement of gold in various tissues and organs (Scott and Lillicrap, 1988). The studies have helped in the understanding of how those elements behave in the human body.

Other elements for which *in vivo* measurements have been developed or were proposed include iron (Farquharson and Bradley, 1999, Shukri *et al.*, 1995) and silver (Graham and O' Meara, 2004) in skin phantoms, arsenic in skin (Studinski *et al.*, 2004), strontium in bone (Pejovic-Milic *et al.*, 2004, Zamburlini *et al.*, 2007) and simultaneous determination of iron, zinc and copper in skin phantoms (Bagshaw and Farquharson, 2002, Bradley and Farquharson, 2000). The detection of metallic fragments in the eye (Zeimer *et al.*, 1974), and calcium and bone-seeking elements such as lead, strontium and zinc in tooth enamel (Zaichick *et al.*, 1999) were also reported.

All the studies mentioned above uses the *K* XRF method except Wielopolski *et al*. (1983) who first described the use of *L* XRF method for bone lead measurements. The *L* XRF method uses weakly-penetrating radiation and concentrates on the emissions from the *L*-shell electrons compared to the *K* XRF method which uses radiation that penetrates more deeply and concentrates on the *K*-shell electron emissions. The purpose of using the *L* XRF method was to obtain a lower radiation dose so as to employ the system for lead measurement in children.

2.6 Review of an XRF System

The technique of XRF involves two principal components which are the excitation system and the detection system. The design of an XRF system is composed of several components which include the excitation source, measurement

geometry, collimation, shielding, samples, the detector with electronics, data analysis, calibration and dosimetry.

2.6.1 The Excitation Source

The function of an excitation source is to excite the characteristic X-rays in a sample via the XRF process. The major requirements of an excitation source are that it is stable, efficient and sufficiently energetic to eject an electron from the appropriate atomic level of the atom of the elements of interest. To be efficient, it must yield a high counting rate for each analyte line and also provide a high peak-to-background ratio (Jenkins *et al.*, 1995). There are two types of excitation sources that have been used for *in vivo* analysis, namely a radioactive isotope or an X-ray machine.

An advantage of a radioactive source is the stable output intensity, compared with the X-ray tube output which may vary to some extent over time. A radioactive source is also compact, transportable and requires no power supply. On the other hand, it may have a short half-life, is expensive, emitting radiation of fixed energy only and give a low fluence rate. Radioactive sources are, therefore, not flexible versus energy and not suitable for analysis of low amounts of chemical elements (Tsuji *et al.*, 2004). However, when a radioactive source is used, the choice of radioactive sources depends on the photon energy emitted such that the energy must be greater than, but as close as possible to the *K* absorption edge of the element of interest. In this energy region, the *K*-shell photoelectric cross section of the element is at its highest hence photons with this energy have a high probability of undergoing a photoelectric event when interacting with an atom of the element. The source

should also have a relatively simple energy spectrum, preferably mono-energetic to minimise the background due to scattered radiation in the energy region of the fluorescence peaks of the element. Radioactive sources such as ^{241}Am, ^{57}Co, ^{125}I, ^{109}Cd and ^{133}Xe have been used for the production of the characteristic X-rays of the various elements. ^{241}Am has been used as an excitation source where it benefits from the 26.3 keV γ-rays emitted to generate the characteristic X-rays of ^{109}Cd ($K\alpha_1$ = 23.1 keV) in the kidney and liver (Ahlgren and Mattsson, 1981) and the 59.5 keV γ-rays emitted to generate the characteristic X-rays of iodine ($K\alpha_1$ = 28.5 keV) for the determination of concentration and elimination rate of iodine-containing contrast agent from living tissue of rabbits (Gronberg *et al.*, 1981). The primary photon energy of 122 keV from ^{57}Co was used to excite lead in finger bone (Ahlgren *et al.*, 1976) and uranium with *K* absorption edge of 115.6 keV in bone phantoms (O' Meara *et al.*, 1997). ^{125}I has been used as the excitation source to measure the soft *L* X-rays emitted from lead in the bone (Wielopolski *et al.*, 1983), *K* X-rays of strontium in bone (Zamburlini *et al.*, 2007) and silver in silver-doped skin phantoms (Graham and O' Meara, 2004). For bone lead measurements, ^{109}Cd source is the most widely used compared to ^{57}Co and ^{125}I sources. The 88 keV γ-rays from ^{109}Cd was used to excite the *K* X-rays of lead (Aro *et al.*, 1994, Green *et al.*, 1993, Laird *et al.*, 1982, Somervaille *et al.*, 1985). ^{109}Cd was also used to excite other elements such as arsenic (Studinski *et al.*, 2004) and iron (Shukri *et al.*, 1995) in skin phantoms, cadmium in bone phantoms (Popovic *et al.*, 2006) and bone strontium (Pejovic-Milic *et al.*, 2004) based upon the 22.1 keV silver X-rays emitted by the source. The feasibility of measuring mercury in the kidney with ^{109}Cd was also carried out (Grinyer *et al.*, 2007). The potential of ^{133}Xe as an excitation source was studied for the *in vivo* X-ray fluorescence of gold (Scott and Lillicrap, 1988) and platinum (Ogg

et al., 1994). The disadvantages of using ^{133}Xe are it has a short half-life (5.25 days); and because it is a gas it is difficult to obtain in high-activity concentrations, hence a high counting time of 92 minutes was used due to the low activity of the ^{133}Xe source (Scott and Lillicrap, 1988).

X-ray tubes have been used ever since Roentgen's discovery of the new kind of radiation in 1895, and they have been developed into remarkably reliable and useful devices. Employing an X-ray tube would reduce the cost and handling difficulties associated with the radioactive materials. An X-ray tube source does not decay over time and when switched off it produces no radiation. X-ray generators are also easy to control and operate. For specific applications requiring a rather narrow range of performance, excitation by radioactive source is convenient but for a broad range of capability, an X-ray tube is usually employed (Jenkins et al., 1995). X-ray tubes have been used for the *in vivo* XRF measurements with different operating voltages and operating currents and anode material. An X-ray tube operated from 70 to 300 kV was used to excite platinum in the head and neck tumours (Ali *et al.*, 1998b). For the excitation of platinum in the kidney of *Cisplatin*-treated patients, X-ray tubes operated at 155 kV and 25 mA (Jonson *et al.*, 1988) and 220 kV (Kadhim *et al.*, 2000) were used. A tungsten anode X-ray tube operated at 150 kV and 15 mA was used as the source for excitation of cadmium in the kidney (Christoffersson and Mattsson, 1983) and at 160 kVp and 0.5 mA was employed for the *in vivo* XRF measurements of kidney and liver cadmium (Borjesson *et al.*, 2000). A molybdenum target X-ray tube operated at 35 kV and 0.8 mA was employed to measure arsenic in superficial layers of tissue-simulating phantoms (Studinski *et al.*, 2006). Mercury kidney and liver measurements were performed with an X-ray generator operated at

160 kV and 20 mA, while a current of 10 mA was used for the thyroid measurements (Borjesson *et al.*, 1995) and at 250 kV and 15 mA for measuring kidney mercury (O' Meara *et al.*, 2000). A tungsten target X-ray tube operated at 20 kV and 20 mA was used to determine the concentration of iron in skin phantoms (Farquharson and Bradley, 1999) and at 40 kV and 5 mA (Bagshaw and Farquharson, 2002) and 15 kVp and 23 mA (Bradley and Farquharson, 2000) for the evaluation of iron, copper and zinc in skin phantoms while an X-ray tube operated at 50 kVp and 30 mA was used to excite the bone lead *L* X-rays (Wielopolski *et al.*, 1989).

2.6.2 Measurement Geometry

In the design of an excitation system, the principal aim is to obtain the optimal ratio of fluorescence to scattering. For this purpose the angle between the excitation radiation and the sample should be chosen as to obtain Compton scattering with a maximum energy below the energy of the fluorescence X-ray to be measured. A number of special configurations have been used by different workers in order to solve specific analytical problems.

When an X-ray tube source is used for excitation, the detector is placed at 90° on the other side of the source (Ali *et al.*, 1998a, Christoffersson and Mattsson, 1983, Farquharson and Bradley, 1999, Lewis, 1994, Pejovic-Milic *et al.*, 2004, Studinski *et al.*, 2006). On the other hand when a radioisotope source is used, a 180° or backscatter geometry is the preferred arrangement of the source-detector assembly (Green *et al.*, 1993, Grinyer *et al.*, 2007, O' Meara *et al.*, 1997, O' Meara *et al.*, 1998b, Ogg *et al.*, 1994, Scott and Lillicrap, 1988, Shukri *et al.*, 1995, Somervaille *et al.*, 1985, Zamburlini *et al.*, 2007) although the 90° geometry have also been applied

(Graham and O' Meara, 2004, Pejovic-Milic *et al.*, 2004). The backscatter geometry is preferable compared to the 90° geometry as it offers minimum attenuation by overlying sample since both incident and outgoing photons are approximately normal to the sample surface (O' Meara *et al.*, 1997) and it allows a more precise and reliable positioning during measurement (Zamburlini *et al.*, 2007). The 90° geometry gives a lower detection limit as compared to the backscatter geometry for the measurement of arsenic in skin phantoms when both configurations were employed using ^{109}Cd as the excitation source (Studinski *et al.*, 2004).

2.6.3 Collimation and Shielding

A source collimator and a detector collimator would define the solid angle subtended by the source and the detector respectively. The source need to be collimated to minimise the beam's divergence and the detector needs to be collimated and shielded to reduce the detection of unwanted scattered radiation which would reduce the signal-to-noise ratio. The subject and user also need to be shielded from the scattered radiation. The total collimation in an experimental system is a compromise between having a low count rate arising from too much detector collimation and a deterioration in the signal-to-noise ratio due to insufficient detector collimation, which produces a broad Compton peak and hence a high scatter contribution under the element fluorescence peaks (Scott and Lillicrap, 1988). To maximise the sensitivity of an XRF system, the collimation and the source-to-sample distance (SSD) should be selected such that the volume irradiated by the source coincides with the volume viewed by the detector. This reduces unnecessary dose to the subject and minimises the energy range and intensity of the detected Compton scattered photons (O' Meara *et al.*, 1997, Somervaille *et al.*, 1985).

Collimators that have been used for the *in vivo* XRF studies come in several shapes and sizes and the collimator material depends on the element of interest. A detector collimator made of copper was used instead of lead to reduce the detection limit for platinum (Jonson *et al.*, 1988) and tungsten was employed for having characteristic X-rays well separated from that of lead and also to maximise photon attenuation (Somervaille *et al.*, 1985). Other researchers used brass with an inner diameter of 25 mm (Ali *et al.*, 1998b) and lead with an opening diameter of 15 mm (Christoffersson and Mattsson, 1983). When a radioactive source is used, the source collimator is constructed to also function as a source holder; such as ^{125}I sources placed inside a molybdenum collimator (Studinski *et al.*, 2005) and a titanium holder/collimator (Graham and O' Meara, 2004), a ^{57}Co source was placed inside a tungsten source holder (O' Meara *et al.*, 1997) and a ^{109}Cd source in a tungsten collimator (Grinyer *et al.*, 2007). For collimation of the primary and scattered beams, a brass tube of length 250 mm and 25 mm in diameter (Jonson *et al.*, 1988), lead (Gronberg *et al.*, 1981), lead cylinders of an inner diameter of 25 mm (Christoffersson and Mattsson, 1983) and stainless steel tubes of lengths 125 mm and 250 mm and both with its inner and outer diameters of 25 mm and 45 mm respectively (Ali *et al.*, 1998b) were used.

2.6.4 Phantoms

A good phantom or sample preparation is a key factor in obtaining reliable, precise, and representative results using XRF techniques. The shape and materials of the phantoms used by researchers differ according to the specific part of the body to be analysed such as the tibia, finger, bone, kidney, skin, liver etc. The calibration phantoms were constructed or fabricated from different materials to which the

element to be determined is added in order to allow quantitative measurements to be taken. The final sample must contain all the elements that are present in the initial material and be homogenously distributed in their true concentration levels. Kidney phantoms filled with solutions of the element of interest that have been used includes a thin-walled Perspex cylinder of height 110 mm and an inner diameter of 40 mm (Ahlgren and Mattsson, 1981, Christoffersson and Mattsson, 1983), a Perspex cylinder of diameter 40 mm placed at a medial distance of 50 mm and at a depth of 50 mm in a water filled bath (Jonson *et al.*, 1988), a polyethylene water tank (Grinyer *et al.*, 2007), a polythene bottle of diameter 48 mm (Scott and Lillicrap, 1988) and a polyethylene bottle of height 80 mm and 48 mm in diameter submerged in a water tank (O' Meara *et al.*, 2000). Liver phantoms used are thin-walled Perspex parallelepipeds with dimensions of 150 mm × 150 mm × 60 mm (Ahlgren and Mattsson, 1981) and the finger phantoms were in the shape of cylinders of length 50 mm and diameter 20 mm made from silica paraffin wax due to easy handling and acceptable radiophysical properties (Ahlgren and Mattsson, 1979).

Plaster of Paris $\left(CaSO_4.\frac{1}{2}H_2O\right)$ was the standard material used to simulate bone in the XRF system and was used as bone phantoms (Carew *et al.*, 2005, O' Meara *et al.*, 1998b, Pejovic-Milic *et al.*, 2004, Popovic *et al.*, 2006, Somervaille *et al.*, 1985, Zamburlini *et al.*, 2007). In addition, a commercially available bone equivalent plastic was also used (Pejovic-Milic *et al.*, 2004). Paraffin wax (Popovic *et al.*, 2006) and wax (Carew *et al.*, 2005, Zamburlini *et al.*, 2007) were used to simulate the surrounding soft tissue around the bone. A water filled cylindrical phantom of 30 mm diameter made of Perspex (Ali *et al.*, 1998a) and a 36 mm